Experimental modeling and design optimization of push-pull electret loudspeakers

Mingsian R. Bai[a] and Chun-Jen Wang
Department of Mechanical Engineering, National Chiao-Tung University, 1001 Ta-Hsueh Road, Hsin-Chu 300, Taiwan

Dar-Ming Chiang and Shu-Ru Lin
Taiwan Electrets Electronics Co., Ltd., 7F-3, 9, Prosperity 1st Road, Hsinchu Science Park, Hsinchu City 30078, Taiwan

(Received 9 August 2009; revised 4 December 2009; accepted 3 February 2010)

A fully experimental modeling technique and a design optimization procedure are presented in this paper for push-pull electret loudspeakers. Conventional electrical impedance-based parameter identification methods are not completely applicable to electret speakers due to the extremely weak electromechanical coupling. This prompts the development of an experimental technique for identifying the electroacoustic parameters of the electret speakers. Mechanical parameters are identified from the membrane velocity measured using a laser vibrometer. The voltage-force conversion factor and the motional impedance are estimated, with the aid of a test-box method. This experimentally identified model serves as the simulation platform for predicting the response of the electret loudspeaker and optimizing the design. Optimal parameters are calculated by using the simulated annealing (SA) algorithm to fulfill various design goals and constraints. Either the comprehensive search for various parameters or the simple search for the optimal gap distance can be conducted by this SA procedure. The results reveal that the optimized design has effectively enhanced the performance of the electret loudspeaker.
 [DOI: 10.1121/1.3337224]

PACS number(s): 43.38.Bs, 43.38.Ja, 43.40.Dx [AJZ] Pages: 2274–2281

I. INTRODUCTION

Electret loudspeakers are the electrostatic loudspeakers with precharged membranes. Electret loudspeakers offer advantages of compactness, light weight, excellent mid- and high frequency reproductions, high electroacoustic efficiency, waiver of externally bias circuit, etc.[1] Due to these characteristics, the loudspeakers have promise in the application to consumer electronics.

Electret configuration will result in slightly different forms of voltage-force sensitivity and the associated nonlinearity from those of conventional push-pull electrostatic loudspeakers. Nevertheless, one may equate the electret electrostatic speaker with an external polarizing voltage. On the surface, the two kinds of loudspeaker look alike. Their equivalent electrical circuits are the same and the analyses of their mechanical and acoustical parameters are identical. However, where they differ is in the electromechanical force conversion. A non-electret electrostatic has an external polarizing voltage supply, which creates a monopole charge on the membrane. For an electret speaker this is difficult to achieve because, in the absence of a supply, a monopole charge is relatively unstable over time. Hence, electret speakers typically use membranes with conductive coatings, which carry an induced charge of opposite polarity (dipoles) to that of the membrane. This makes the analysis somewhat more complicated. It turns out that the two kinds of loudspeaker are equivalent but not the same. In the case of the dipole electret, it is like applying a polarizing voltage of an equivalent non-electret speaker across the conductive coating and a virtual electrode somewhere in the middle of the membrane, where this virtual electrode contains all the membrane charge in a concentrated layer. The electrical input capacitance of an electret speaker is also different from that of a non-electret type due to the presence of the electret membrane, although the contribution this makes depends on the size of the air gap.[2,3]

Electret materials have been studied by several researchers. Lekkala and Paajanen[4] introduced a new electret material, electromechanical film (EMFi), at the turn of the century. Not before long, EMFi was applied to microphones, actuators, and even loudspeaker panels.[5] Cao *et al.*[6] discussed the relationship between the microstructures and the properties of the electret material, where the electret properties of the porous polytetrafluoroethylene (PTFE) were studied. It is found that the porous dielectrics can be good electret materials. Recently, Chiang *et al.*[7] proposed the nanoporous Teflon-fluorinated ethylene propylene film that allows for higher charge density stored in the film with improved stability. The nanoporous electret material was applied to flexible electrostatic loudspeakers.[8] Their electret diaphragms are made of fluoro-polymer with nano-meso-micro-pores precharged by the corona method.

It was not until recently that Mellow and Kärkkäinen[3,9] conducted a rigorous theoretical analysis of electret loud-

[a]Author to whom correspondence should be addressed. Electronic mail: msbai@mail.nctu.edu.tw

speakers. Transducers with single-ended and push-pull constructions are investigated in terms of the static force acting on the diaphragm and the stored charge density. Bai *et al.*[10] suggested a hybrid modeling approach combining experimental measurement and finite-element-analysis (FEA) for a single-ended electret loudspeaker. Experimental verification reported in the work revealed that the single-ended loudspeaker suffered from high nonlinear distortion problems.

This paper aims at three purposes. First, electret loudspeakers in push-pull construction are proposed in order to reduce the nonlinear distortions encountered in the single-ended device. Second, a more accurate fully experimental modeling technique is suggested to estimate the lumped parameters of the equivalent circuits without resorting to FEA. Because the coupling between the electrical and mechanical systems is extremely weak, the parameters of the mechanical system are unidentifiable using the electrical impedance measurement.[11–13] To overcome the difficulty, a test-box approach in conjunction with laser measurement is taken in this paper. Third, on the basis of the preceding simulation model, an optimization procedure using simulated annealing (SA) algorithm[14–16] is developed, aiming at optimizing design parameters of electret loudspeakers to maximize the sound pressure level (SPL) output and the bandwidth as well.

II. EXPERIMENTAL MODELING OF ELECTRET LOUDSPEAKERS

A. Operating principles

A sample of a 493×129 mm^2 electret loudspeaker is shown in Fig. 1(a). In its push-pull construction, the loudspeaker comprises a charged flexible membrane and two perforated rigid back plates with 52.1% perforation ratio. The membrane is made of fluoro-polymer, which contains nanopores to enhance the charge stability and density.[8] The membrane is placed at the center between two electrode plates spaced by 2.4 mm, as shown in Fig. 1(b). The construction is also referred to as the push-pull configuration with a fully floating membrane by Mellow and Kärkkäinen.[3] The membrane is divided into six equal partitions (242×37 mm^2) by stainless steel spacers.

Due to high input impedance of the electret loudspeaker, a transformer is used for impedance matching and e_{spk} is the output voltage of the transformer. The turn ratio is 138. The net force f acting on the membrane can be estimated by[3]

$$f=\frac{\varepsilon_r\varepsilon_{r1}hS_D\sigma_m}{2(\varepsilon_r d+\varepsilon_{r1}h)^2}e_{\mathrm{spk}}+\frac{\varepsilon_r\varepsilon_{r1}h^2S_D\sigma_m^2}{2\varepsilon_0(\varepsilon_r d+\varepsilon_{r1}h)^3}\delta=\phi e_{\mathrm{spk}}+\kappa\delta, \tag{1}$$

where ε_r and ε_{r1} are the relative permittivities of the membrane and the medium at the gap, respectively, ε_0 is the vacuum permittivity, h is one-half of the thickness of the membrane, S_D is the area of membrane, σ_m is the surface charge density of the membrane, d is the gap between the membrane and the electrode plate, and δ is the displacement of the membrane. The first term of Eq. (1) is due to the input voltage, whereas the second term is due to the negative stiffness resulting from the membrane attractions. The voltage-force conversion factor ϕ and the negative stiffness κ can be written as[3]

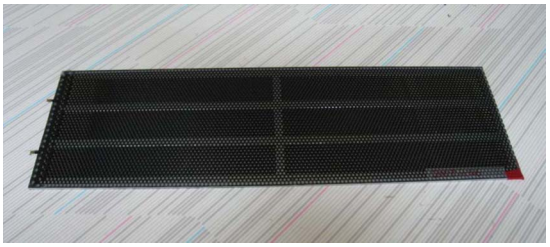

(a)

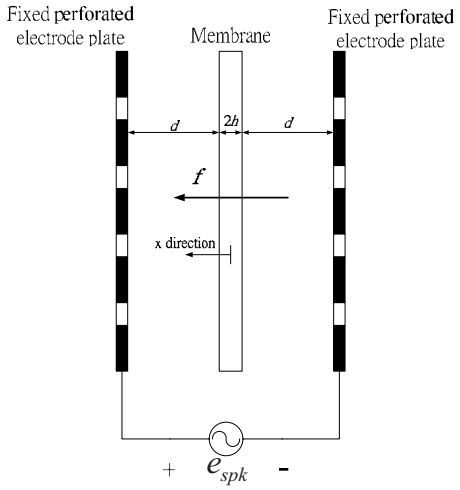

(b)

FIG. 1. (Color online) The push-pull electret loudspeaker. (a) Photo. (b) The schematic of the loudspeaker construction.

$$\phi=\frac{K_1}{d^2},\quad d\gg\frac{\varepsilon_{r1}h}{\varepsilon_r} \tag{2}$$

with $K_1=\varepsilon_{r1}hS_D\sigma_m/2\varepsilon_r$, and

$$\kappa=\frac{K_2}{d^3},\quad d\gg\frac{\varepsilon_{r1}h}{\varepsilon_r} \tag{3}$$

with $K_2=\varepsilon_{r1}h^2S_D\sigma_m^2/2\varepsilon_0\varepsilon_r^2$.

B. Analogous circuits

The electret loudspeaker can be modeled with the analogous circuit, as shown in Fig. 2(a). The mechanical impedance and the radiation impedance are identified as a lumped sum in the parameter identification procedure. That is, the radiation impedance has been taken into account in the modeling. In the electrical domain, the circuit is modeled with the Thévenin equivalent circuit, where e_{in} is the voltage source of the transformer input, i is the current, and R_E and L_E are the electric resistance and inductance of the transformer. C_E is the static capacitance when the membrane is blocked. In the mechanical domain, Z_M represents the open-circuit mechanical impedance and u is the membrane velocity. In the acoustical domain, Z_A represents the acoustical impedance.

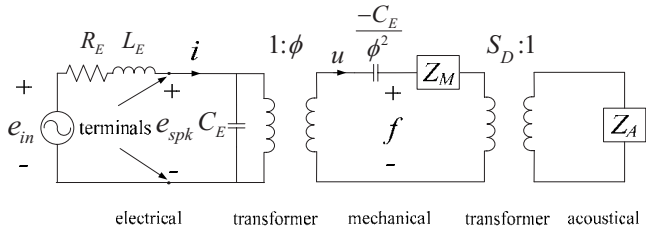

(a)

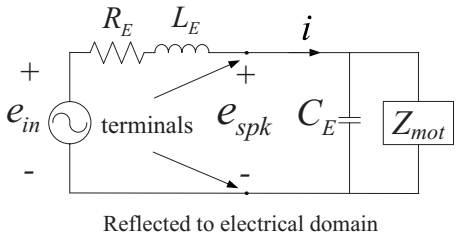

(b)

FIG. 2. The electroacoustic analogous circuits of the push-pull electret loudspeaker. (a) Electrical, mechanical, and acoustics systems. (b) Combined circuit referred to the electrical system.

Figure 2(b) shows the combined circuit as the mechanical and acoustical systems are reflected to the electrical system, where the motional impedance Z_{mot} is defined as

$$Z_{\text{mot}} = \frac{Z_{ms} + S_D^2 Z_A}{\phi^2}, \tag{4}$$

$$Z_{ms} = Z_M - \left(j\omega \frac{C_E}{\phi^2}\right)^{-1}, \tag{5}$$

where Z_{ms} is the short-circuit mechanical impedance and ω is the angular frequency. To measure the electrical impedance, we need an experimental arrangement, as shown in Fig. 3(a). The input voltage from the signal generator e_g is 1.5 V and the current-sampling resistor R is 100 Ω. The electrical impedance of the loudspeaker is given by

$$Z_{\text{spk}} = \frac{e_g G_1 G_2 - e_R}{e_R} R, \tag{6}$$

where G_1 and G_2 denote the effective gains of the amplifier and the transformer, respectively, and e_R is the voltage drop across the resistor R. The thus measured electrical impedance of Fig. 3(b) resembles that of a capacitance due to weak electromechanical coupling[10]

$$|Z_E| = (\omega C_E)^{-1}. \tag{7}$$

It follows that only the static capacitance C_E can be extracted from the electrical impedance measurement

$$C_E = (\omega |Z_E|)^{-1}. \tag{8}$$

For the sample in Fig. 1, the C_E was found to be 1.86 nF.

C. Parameter identification

In Fig. 2(b), as the inductance L_E of the transformer output end is connected to the electret loudspeaker, which behaves like a capacitance due to the aforementioned weak

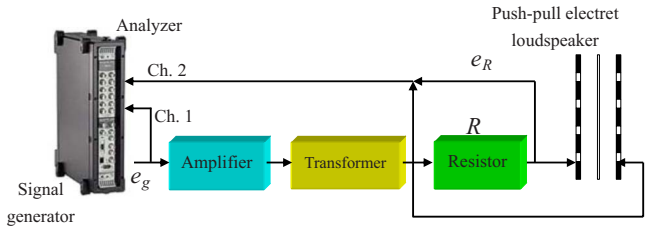

(a)

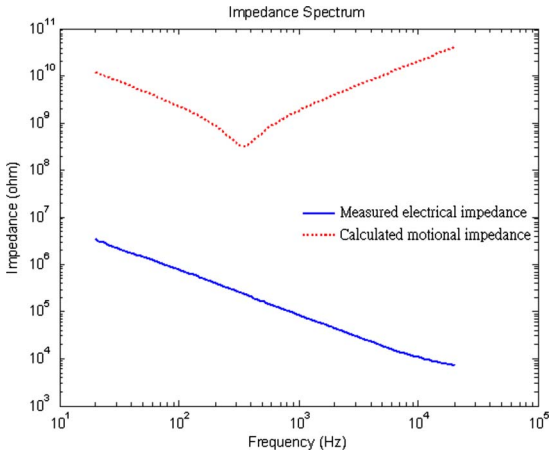

(b)

FIG. 3. (Color online) The electrical impedance measurement of the push-pull electret loudspeaker. (a) Experimental arrangement. (b) The electrical impedance versus the motional impedance.

coupling, the combined electrical system becomes a second-order low-pass system. Figure 4 shows the frequency response of the unloaded transformer, which is nearly constant throughout the range 20–20 kHz. As the electret loudspeaker is connected to the transformer, the frequency response becomes a low-pass function with cutoff frequency ω_{E0} =8736.4 Hz as follows:

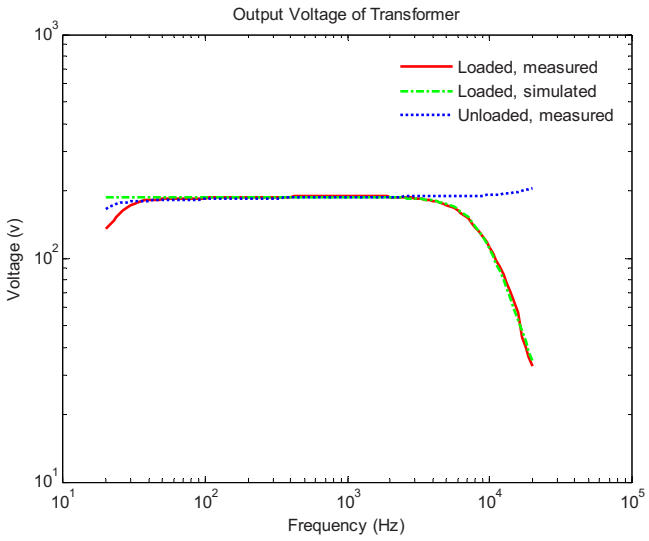

FIG. 4. (Color online) The comparison of the measured and simulated output voltage responses of the loaded and unloaded transformers.

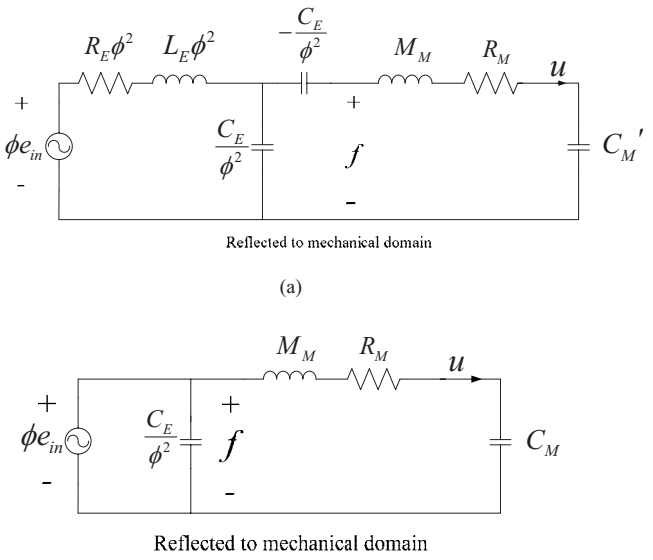

FIG. 5. The electroacoustic analogous circuits of the push-pull electret loudspeaker. (a) Combined circuit referred to the mechanical system. (b) The weakly coupled approximation.

$$e_{\text{spk}}(s) = H(s)e_{\text{in}}(s) = \frac{1}{C_E L_E s^2 + C_E R_E s + 1} e_{\text{in}}(s)$$

$$= \frac{1}{\left(\frac{s}{\omega_{E0}}\right)^2 + \frac{1}{Q_E}\frac{s}{\omega_{E0}} + 1} e_{\text{in}}(s), \tag{9}$$

where $H(s)$ is the transfer function between e_{spk} and e_{in}, Q_E is the quality factor, and $s=j\omega$ is the Laplace variable. The effective inductance and resistance at the output end of the transformer can be calculated by

$$L_E = (\omega_{E0}^2 C_E)^{-1}, \tag{10}$$

$$R_E = (Q_E \omega_{E0} C_E)^{-1}. \tag{11}$$

At the resonance frequency, the real part of the transfer function in Eq. (9) is zero. It follows that the quality factor can be calculated by

$$|H(j\omega_{E0})| = |-jQ_E| = Q_E. \tag{12}$$

For the sample in Fig. 1, the quality factor Q_E=0.6845, the inductance L_E=0.178 H, and the resistance R_E=14.3 kΩ, respectively. In Fig. 4, the measurement (solid line) and the simulation (dashed-dotted line) of e_{spk} are in good agreement. The cutoff frequency is measured according to the phase switching principle.

As mentioned previously, the mechanical parameters are unidentifiable with the electrical impedance measurement. We need to devise a method based on direct mechanical measurement. To this end, the electrical and acoustical systems are reflected to the mechanical system, as shown in Fig. 5(a). For simplicity, we approximate the combined acoustical impedance and the mechanical impedance to be a second-order system. The lumped parameters R_M, M_M, and C_M' denote the resistance, the mass, and the compliance, respectively, of the combined impedance.

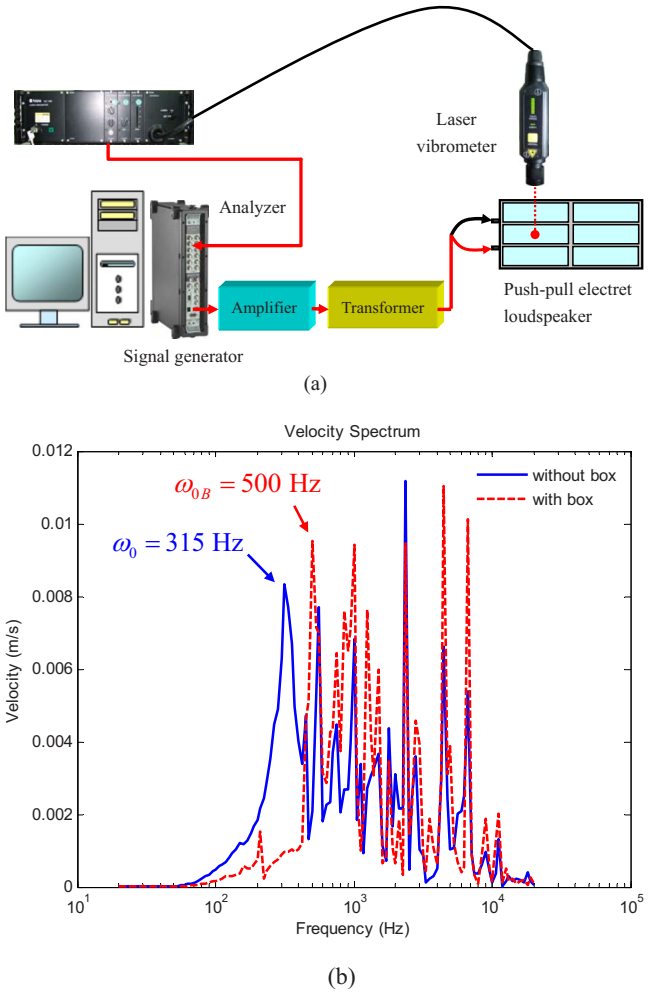

FIG. 6. (Color online) The membrane velocity measurement of the push-pull electret loudspeaker. (a) Experimental arrangement. (b) The comparison of the velocity responses of the loudspeaker, with and without the test box.

Due to weak coupling ($\phi \approx 0$), $R_E\phi^2$ and $L_E\phi^2$ can be neglected, leading to the simplified circuit of Fig. 5(b). Solving the circuit yields the expression of the membrane velocity u as follows:

$$u = \frac{C_M s}{M_M C_M s^2 + R_M C_M s + 1} \phi e_{\text{in}}$$

$$= \frac{1}{R_M} \frac{\frac{1}{Q_u}\left(\frac{s}{\omega_0}\right)}{\left(\frac{s}{\omega_0}\right)^2 + \frac{1}{Q_u}\left(\frac{s}{\omega_0}\right) + 1} \phi e_{\text{in}}, \tag{13}$$

where the compliance C_M is the series combination of C_M' and the negative compliance $-C_E/\phi^2$, ω_0 is the fundamental resonance frequency, and Q_u is the quality factor. The membrane velocity can be measured by a laser vibrometer, as shown in Fig. 6(a). In the following, we concentrate on only the fundamental mode and ignore higher-order modes. From the velocity measurement, the fundamental resonance frequency ω_0 can be located and the quality factor corresponding to the fundamental resonance can be estimated as follows:

$$Q_u = \frac{\omega_0}{\omega_2 - \omega_1}, \tag{14}$$

where the ω_2 and ω_1 are -3 dB points in the velocity response.

Given the $\omega_0 = 1/\sqrt{M_M C_M}$, it is impossible to determine the respective values of the compliance C_M and the mass M_M based on one measurement. To overcome the difficulty, a test-box method with volume 5.51 l is employed to obtain another velocity measurement. The result of the membrane velocity measurement is shown in Fig. 6(b). The fundamental resonance frequency is increased from 315 to 500 Hz due to the acoustical compliance of the test box. The additive acoustical compliance C_{AB} and the additive mechanical compliance ΔC_M due to the test box can be calculated as

$$C_{AB} = \frac{V_{\text{box}}}{\rho c^2}, \tag{15}$$

$$\Delta C_M = \frac{C_{AB}}{S_D^2}, \tag{16}$$

where V_{box} is the volume of the test box, ρ is the density of air, and c is the velocity of sound. Thus, based on these two membrane velocity measurements, the mechanical parameters can be determined as

$$C_M = \left[\left(\frac{\omega_{0B}}{\omega_0}\right)^2 - 1\right]\Delta C_M, \tag{17}$$

$$M_M = (\omega_0{}^2 C_M)^{-1}, \tag{18}$$

$$R_M = (\omega_0 Q_u C_M)^{-1}, \tag{19}$$

$$C_M' = \frac{C_M\left(\frac{C_E}{\phi^2}\right)}{C_M + \frac{C_E}{\phi^2}}, \tag{20}$$

where ω_{0B} is the fundamental resonance frequency of the velocity response when loaded with the test box and ΔC_M is the additive mechanical compliance due to the test box. Finally, the voltage-force conversion factor ϕ can be determined by letting $\omega = \omega_0$ in Eq. (13) as follows:

$$\phi = \frac{R_M u(\omega_0)}{e_{\text{in}}}, \tag{21}$$

where $u(\omega_0)$ is the peak magnitude of the membrane velocity response at the fundamental resonance frequency. Using the formula, ϕ is found to be 1.88×10^{-4} for the sample in Fig. 1.

D. Numerical and experimental investigations

Experiments were conducted to validate the preceding model of the electret loudspeaker. The experimental arrangement for measuring the on-axis SPL is shown in Fig. 7(a). According to the standard AES2-1984 (r2003),[17] a 2475 $\times$ 2025 mm^2 baffle is used in the measurement. The 132.6 Vrms swept-sine signal is used to drive the loudspeaker in the frequency range 20–20 kHz. The microphone is positioned 1 m away from the loudspeaker.

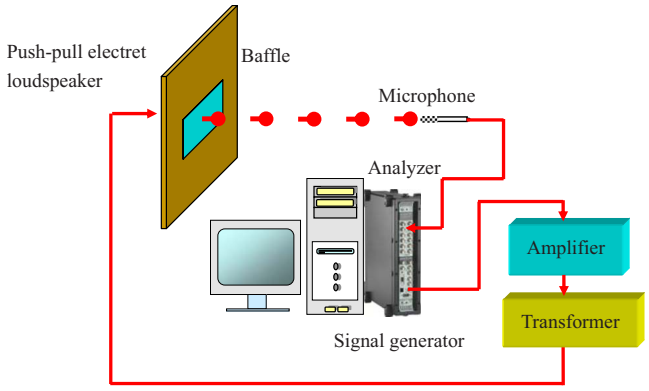

(a)

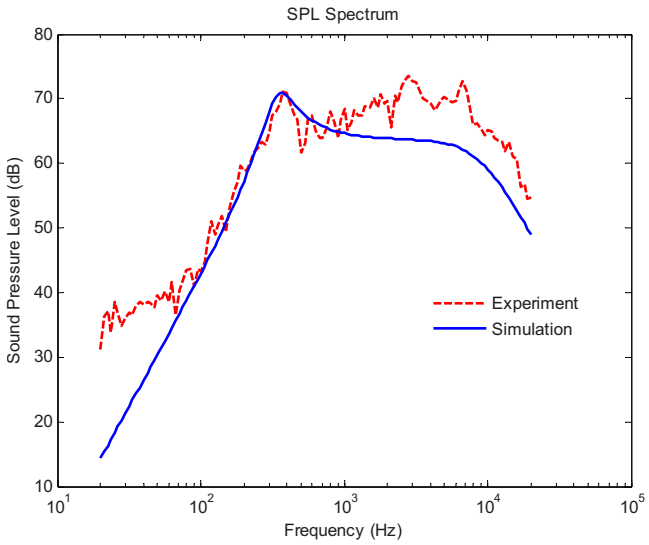

(b)

FIG. 7. (Color online) The on-axis SPL measurement of the push-pull electret loudspeaker. (a) Experimental arrangement. (b) The comparison of the measured and the simulated on-axis SPL responses.

Figure 7(b) compares the on-axis SPL responses obtained using the simulation and the measurement. The simulated response (solid line) is in good agreement with the measured response (dashed line), albeit discrepancies are seen at high frequencies due to un-modeled flexural modes of membrane. It should be borne in mind that, in the preceding model, only the fundamental mode is modeled in the analogous circuit and high-order modes are neglected.

It can also be observed from Fig. 7(b) that the SPL response starts to roll off at approximately 8 kHz due to the inductance of the transformer as predicted. Furthermore, in Fig. 3(b), the motional impedance obtained using the model is much greater than the electrical impedance, rendering the former an open circuit in Fig. 2(b). This is the evidence of weak coupling.

For assessing the nonlinear distortion of the electret loudspeaker, total harmonic distortion (THD) is calculated from the measured on-axis SPL response.[18] In Fig. 8, the

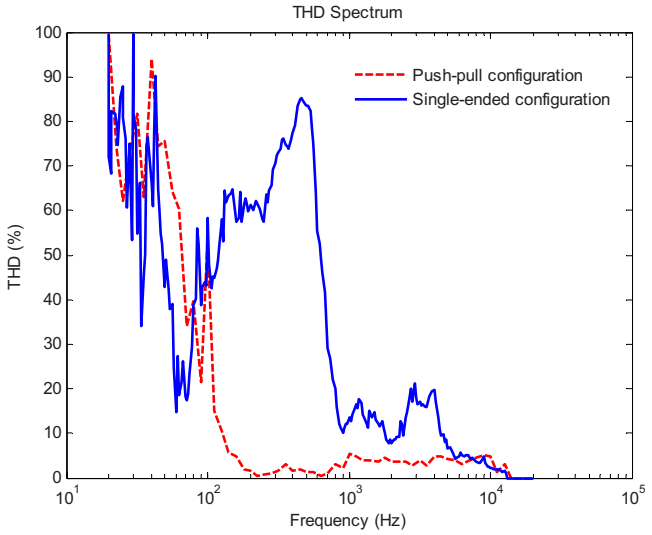

FIG. 8. (Color online) The comparison of the measured THD of the electret loudspeaker between the push-pull and the single-ended configurations.

measured THD of the electret loudspeaker in push-pull construction is compared with that of the single-ended construction, which was investigated by Bai *et al.*[10] The average THD of the push-pull configuration is below 6% in the range 140–20 kHz, while the THD of the single-ended configuration can reach as high as 17%. Evidently, the push-pull configuration has effectively addressed the nonlinearity problem of the single-ended configuration.

III. PARAMETER OPTIMIZATION OF ELECTRET LOUDSPEAKERS

The preceding model of electret loudspeaker serves as a useful simulation platform for optimizing the loudspeaker parameters. In the following, a procedure based on the simulated annealing (SA) algorithm[14–16] is exploited for the design optimization.

A. The SA algorithm

The SA algorithm is a generic probabilistic meta-algorithm for the global optimization problem, namely, locating a good approximation to the global optimum of a given function in a large search space. The major advantage of the SA is the ability to avoid becoming trapped in the local minima. In the SA method, each state in the search space is analogous to the thermal state of the material annealing process. The objective function G is analogous to the energy of the system in that state. The purpose of the search is to bring the system from the initial state to a randomly generated state with the minimum objective function. An improve state is accepted in two conditions. If the objective function is decreased, the new state is always accepted. If the objective function is increased and the following inequality holds, the new state will be accepted:[16]

$$P = \exp\left(-\frac{\Delta G}{T}\right) > \gamma, \tag{22}$$

where P is the acceptance probability function, ΔG is the difference of objective function between the current and the previous states, T is the current system temperature, and γ is a random number, which is generated in the interval (0,1). In the high temperature T, there is high probability P to accept a new state that is "worse" than the present one. This mechanism prevents the search from being trapped in a local minimum. As the annealing process goes on and T decreases, the probability P becomes increasingly small until the system converges to a stable solution. The annealing process begins at the initial temperature T_i and proceeds with temperature that is decreased in steps according to

$$T_{k+1} = \alpha T_k, \tag{23}$$

where $0 < \alpha < 1$ is a annealing coefficient. The SA algorithm is terminated at the preset final temperature T_f. In the electret loudspeaker optimization, we choose $T_i = 1000$, $T_f = 1 \times 10^{-9}$, and $\alpha = 0.95$. Next, two design optimization problems will be examined. The first problem concentrates on only optimizing the gap distance d between the membrane and the electrode plate, whereas the second problem attempts to optimize four design parameters: the gap distance d, the compliance C'_M, the mass M_M, and the resistance R_M.

B. Optimizing the gap distance

In the section, only the gap distance that is easiest to alter in making a mockup will be optimized. If all other conditions remain unchanged, the net attraction force acting on the membrane and hence the SPL output will increase as the gap is decreased. However, the gap cannot be reduced indefinitely, or else, stick-up condition of the membrane and the electrode plates can occur. Another issue is that the upper roll-off frequency will also become lower (because of the increased static capacitance) as the gap is decreased.

As we keep decreasing the gap to increase the attraction force until the displacement of the membrane equals the gap distance, we call this distance the critical gap distance. Only dynamic distance needs to be concerned since, at the quiescent state, the static attraction forces due to resident charges in the membrane are balanced with the push-pull construction. Membrane displacement can be obtained by integrating the velocity expression in Eq. (13) as follows:

$$\delta = \frac{u}{s} = \frac{K_1}{R_M Q_u \omega_0} \frac{1}{\left(\frac{s}{\omega_0}\right)^2 + \frac{1}{Q_u}\left(\frac{s}{\omega_0}\right) + 1} \frac{e_{\text{in}}}{d^2}, \tag{24}$$

where $\phi = K_1/d^2$ in Eq. (2) has been invoked. The collision condition occurs when the peak value of the displacement $|\delta|_{\max}$ is equal to the gap distance d. This gives the critical gap distance

$$d^* = \left\{ \frac{K_1}{R_M Q_u \omega_0} \frac{Q_u^2}{\sqrt{Q_u^2 - 0.25}} |e_{\text{in}}| \right\}^{1/3}. \tag{25}$$

In the experiment, the driving signal is a 132.6 Vrms swept sine. That corresponds to a critical gap distance 0.19 mm, which also represents an upper bound of displacement for the following optimization. Figure 9(a) compares the SPL responses for various gap distances (including the critical gap). Clearly, the SPL is increased if the gap distance is decreased.

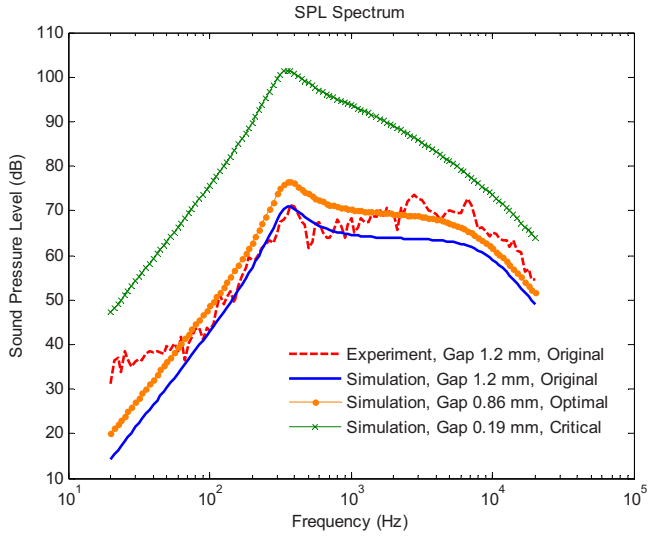

(a)

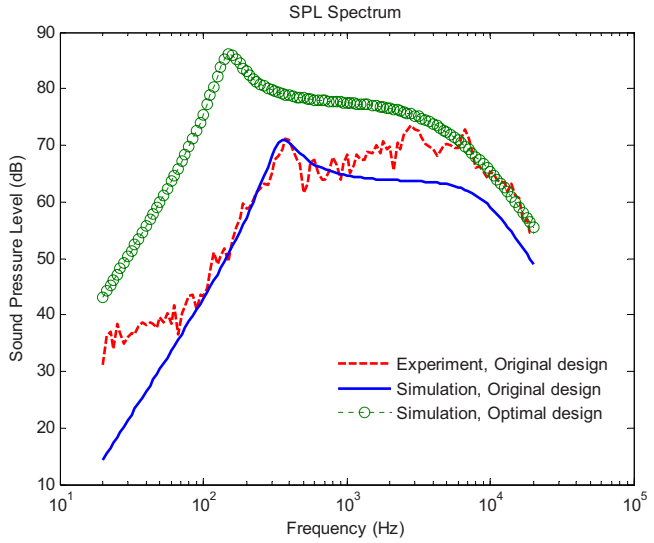

(b)

FIG. 9. (Color online) The comparison of the on-axis SPL responses between the original and the optimal designs. (a) Results of optimizing only the gap distance. (b) Results of optimizing four parameters including the gap distance, the resistance, the mass, and the compliance.

However, this comes at the expense of decreased bandwidth due to increased static capacitance.

In order to find a compromise solution between the original design and the design with the critical gap, the SA algorithm is employed alongside the preceding simulation model for finding the optimal gap distance. Two goals are set up for the design optimization. It is hoped that the SPL in the range 800–5 kHz is maximized while maximizing the upper roll-off frequency, i.e.,

$$G_1 = \sqrt{\frac{1}{N}\sum_{n=1}^{N} (\mathrm{SPL}_{\mathrm{new}}(n))^2}, \quad f(n) \in [800\ \mathrm{Hz}, 5\ \mathrm{kHz}],$$
$$n = 1, \ldots, N, \tag{26}$$

TABLE I. Parameters of the optimized design versus the original non-optimized design.

	R_M (N s/m)	C'_M (m/N)	M_M (kg)	Gap (mm)
Original (1)	3.47	1.95×10^{-5}	1.17×10^{-2}	1.2
Optimal (2)	4.0	1.03×10^{-4}	1.1×10^{-2}	0.55
(2)/(1)%	115.44	528.21	94.83	45.83

$$G_2 = f_{\mathrm{uc}}, \tag{27}$$

where $\mathrm{SPL}_{\mathrm{new}}$ is the current SPL response, n is the frequency index in the range 800–5 kHz, and f_{uc} is the upper -3 dB cutoff frequency of $\mathrm{SPL}_{\mathrm{new}}$. The compound objective function G_{TG} can be written as

$$G_{TG} = \frac{1}{G_1} + w \times \frac{1}{G_2}, \tag{28}$$

where w is a weighting constant ($w=0.23$ in the simulation). In addition, the design variable (gap distance) and the associated constraints are given in the following inequalities:

$$0.4\ \mathrm{mm} < d < 2.0\ \mathrm{mm},$$
$$|\delta|_{\max}(\mathrm{mm}) < d(\mathrm{mm}). \tag{29}$$

With the SA procedure, the optimal gap distance is found to be 0.86 mm, which enhances the average SPL by approximately 5 dB, as shown in Fig. 9(a).

C. Optimizing multi-parameters

In the section, we shall extend the preceding one-parameter optimization to more comprehensive optimization for four parameters: the gap distance, the resistance R_M, the mass M_M, and the compliance C'_M. Apart from the level and the upper cutoff design goals, a third goal of the lower cutoff is added to the objective function

$$G_3 = f_{\mathrm{lc}}, \tag{30}$$

where f_{lc} denotes the lower -3 dB cutoff frequency of $\mathrm{SPL}_{\mathrm{new}}$. The compound objective function G_{TM} reads

$$G_{TM} = w_1 \times \frac{1}{G_1} + w_2 \times \frac{1}{G_2} + G_3, \tag{31}$$

where the weights $w_1=2400$ and $w_2=150\,000$ in the simulation. The design variables and the associated constraints are given in the following inequalities:

$$0.698\ \mathrm{N\ s/m} \le R_M \le 69.8\ \mathrm{N\ s/m},$$
$$1.4\times10^{-3}\ \mathrm{kg} \le M_M \le 1.43\times10^{-1}\ \mathrm{kg},$$
$$1.95\times10^{-6}\ \mathrm{m/N} \le C'_M \le 1.95\times10^{-4}\ \mathrm{m/N},$$
$$0.4\ \mathrm{mm} \le d \le 2.0\ \mathrm{mm},$$
$$|\delta|_{\max}(\mathrm{mm}) < d(\mathrm{mm}). \tag{32}$$

The results of optimization using the SA algorithm are summarized in Table I. The design with optimized parameters is

simulated in Fig. 9(b). The lower cutoff frequency of the optimal design (circled mark) has been decreased from 315 Hz of the original design to 150 Hz as the mechanical compliance is increased by 528%. The average SPL is enhanced by about 12 dB as the gap is decreased to 0.55 mm.

IV. CONCLUSIONS

A fully experimental modeling technique and an optimization procedure have been developed in this work for push-pull electret loudspeakers. The experimental modeling technique relies on not only the electrical impedance measurement but also the membrane velocity measured by using a laser vibrometer. With the aid of a test box, the voltage-force conversion factor and characteristics of motional impedance can be identified from the membrane velocity. One of the most important contributions of the present work is that it verifies the theory and proves the linearity of the transduction. The experimentally identified model serves as the simulation platform for optimizing the design parameters of the electret loudspeaker. The SA algorithm was exploited to find the parameters that yield optimal level-bandwidth performance. Either only the gap distance or the comprehensive search for various parameters can be optimized by using the SA procedure. The results reveal that the optimized design has effectively enhanced the performance of the electret loudspeaker, as compared to the original design. In addition, a high-quality audio transformer with wider bandwidth may further enhance the performance and ease the optimization limitations. The search of such transformers is included in the list of action items of future work.

ACKNOWLEDGMENTS

The work was supported by the National Science Council of Taiwan, under Project No. NSC 95-2221-E-009-009-MY2. Special thanks also go to the Material and Chemical Research Laboratories, Industrial Technology Research Institute (ITRI) in Taiwan.

[1] P. J. Baxandall, "Electrostatic loudspeakers," in *Loudspeaker and Headphone Handbook*, 3rd ed., edited by J. Borwick (Focal, Oxford, 2001).
[2] F. V. Hunt, *Electroacoustics: The Analysis of Transduction, and Its Historical Background* (American Institute of Physics, Melville, NY, 1982).
[3] T. Mellow and L. Kärkkäinen, "On the forces in single-ended and push-pull electret transducers," J. Acoust. Soc. Am. **124**, 1497–1504 (2008).
[4] J. Lekkala and M. Paajanen, "EMFi—New electret material for sensors and actuators," IEEE Tenth International Symposium on Electrets, Athens, Greece (1999).
[5] M. Paajanen, J. Lekkala, and K. Kirjavainen, "Electromechanical film (EMFi)—A new multipurpose electret material," Sens. Actuators, A **84**, 95–102 (2000).
[6] Y. Cao, Z. Xia, Q. Lin, J. Shen, L. Chen, and B. Zhou, "Study of porous dielectrics as electret materials," IEEE Trans. Dielectr. Electr. Insul. **5**, 58–62 (1998).
[7] D. M. Chiang, W. L. Liu, J. L. Chen, and R. Susuki, "PALS and SPM/EFM investigation of charged nanoporous electret films," Chem. Phys. Lett. **412**, 50–54 (2005).
[8] D. M. Chiang and J. L. Chen, "A novel flexible loudspeaker driven by an electret diaphragm," AES 121st Convention, San Francisco, CA (2006).
[9] T. Mellow and L. Kärkkäinen, "On the sound field of a circular membrane in free space and an infinite baffle," J. Acoust. Soc. Am. **120**, 2460–2477 (2006).
[10] M. R. Bai, R. L. Chen, and C. J. Wang, "Electroacoustic analysis of an electret loudspeaker using combined finite-element and lumped-parameter models," J. Acoust. Soc. Am. **125**, 3632–3640 (2009).
[11] H. Olson, *Acoustical Engineering* (Van Nostrand, New York, 1957), reprinted by Professional Audio Journals (Philadelphia, PA, 1991).
[12] L. L. Beranek, *Acoustics* (Acoustical Society of America, Melville, NY, 1996).
[13] W. M. Leach, Jr., *Introduction to Electroacoustics and Audio Amplifier Design* (Kendall-Hunt, Dubuque, IA, 2003).
[14] N. Metropolis, A. W. Rosenbluth, M. N. Rosenbluth, A. H. Teller, and E. Teller, "Equations of state calculations by fast computing machines," J. Chem. Phys. **21**, 1087–1092 (1953).
[15] *Quantum Annealing and Related Optimization Methods*, edited by A. Das and B. K. Chakrabarti (Springer, Heidelberg, 2005).
[16] J. de Vicente, J. Lanchares, and R. Hermida, "Placement by thermodynamic simulated annealing," Phys. Lett. A **317**, 415–423 (2003).
[17] Audio Engineering Society Inc., AES Recommended Practice Specification of Loudspeaker Components Used in Professional Audio and Sound Reinforcement, AES2-1984, NY (2003).
[18] M. R. Bai and R. L. Chen, "Optimal design of loudspeaker systems based on sequential quadratic programming (SQP)," J. Audio Eng. Soc. **55**, 44–54 (2007).